2020 IEEE/RSJ International Conference on Intelligent Robots and Systems (IROS)
October 25-29, 2020, Las Vegas, NV, USA (Virtual)

A Compliance Control Method Based on Viscoelastic Model for Position-Controlled Humanoid Robots

Qingqing Li[1], Zhangguo Yu[1,2], Xuechao Chen[1,2], Libo Meng[1,3], Qiang Huang[1,3], Chenglong Fu[4], Ken Chen[5], and Chunjing Tao[6]

***Abstract*— Compliance is important for humanoid robots, especially a position-controlled one, to perform tasks in complicated environments where unexpected or sudden contacts will result in large impacts which may cause instability or destroy the hardware of robots. This paper presents a compliance control method based on viscoelastic model for humanoid robots to survive on these conditions. The viscoelastic model is used to obtain the relationship between the differential of contact force/torque and linear/angular position. Thus a state equation of this model can be established and a state feedback controller adjusting the position to adapt to the contact force/torque can be designed to realize the compliant movement. The proposed compliance control method based on viscoelastic model has been employed in ankle compliance for stable walking on indefinite uneven terrain and arm compliance for falling protection on BHR-6P, a position-controlled humanoid robot, which validates its effectiveness.**

I. INTRODUCTION

Humanoid robots are designed to assist or work in place of human beings on various occasions, such as manufacture, transportation, disaster relief and so on. In order to achieve this goal, the humanoid robot is ought to have the ability of compliance to adapt to the complicated environment with many unexpected or sudden contact impacts.

Compliance can help humanoid robots maintain balance through absorbing impacts caused by external disturbances, unexpected contact, or errors of model and control [1], [2]. In [1] and [3], [4], the authors mounted compliant materials between the foot sole and force sensor on the ankle for position-controlled humanoid robots to realize a compliance behavior, based on which the posture of the trunk could be controlled well. Several compliance control methods also have been developed to improve the stability of the robots, in which the impedance and admittance control [5] are classical compliance methods for torque-controlled and position-controlled robots. In [6], [7] Nakasaka et. al. proposed a Torso Position Compliance Control (TPCC) based on Zero Moment Point (ZMP) and admittance control, which realized the stabilization of dynamic walking and whole-body motion. Similarly, in [8] Caron et. al. used whole-body admittance control to introduce compliance for stable stair climbing at the Airbus factory. In [9], [10], compliance control is also used to maintain balance under external disturbances for humanoid robots.

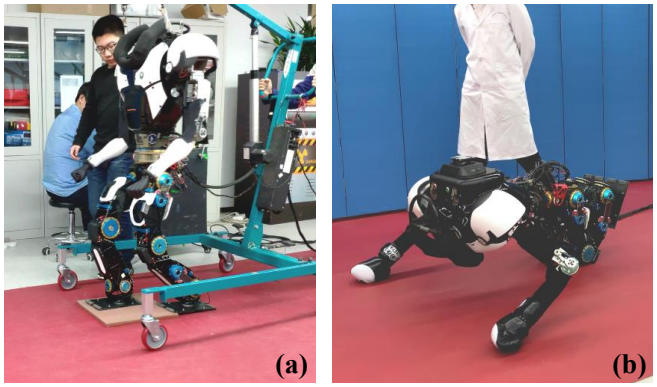

Fig. 1. Applications of compliance control based on viscoelastic model on BHR-6P. (a) Stable walking on indefinite uneven terrain. (b) Arm compliance for falling forward protection.

In recent studies, torque controlled humanoid robots have exhibited notable compliant and dynamic behaviours, such as TORO of DLR [11] and TALOS of PAL [12], [13]. As to position controlled humanoid robots, the compliance is also well performed but not so dynamic and agilely as the torque controlled humanoids does. Thus the impact produced by unexpected or sudden contacts may result in instability or hardware damages to position-controlled humanoid robots more easily.

In this paper, in order to improve the adaptability of position-controlled humanoid robots to large contact impacts, we propose a compliance control method based on viscoelastic model. The viscoelastic model is used to obtain the relationship between the differential of contact force/torque and linear/angular position. Thus a state equation of this model can be established and a state feedback controller adjusting the position to adapt to the contact force/torque can be designed to realize the compliant movement. On occasions of both unexpected and sudden contacts, such as walking on indefinite terrain and falling forwards respectively as shown

This work was supported in part by the National Natural Science Foundation of China under Grant 61533004, Grant 61703043, the Beijing Municipal Science and Technology Project under Grant Z191100008019003, the Beijing Natural Science Foundation under Grant 3192029, and the 111 Project under Grant B08043. (Corresponding author: Zhangguo Yu, yuzg@bit.edu.cn)

[1] School of Mechatronical Engineering, Beijing Institute of Technology, Beijing 100081, China.
[2] Beijing Advanced Innovation Center for Intelligent Robots and Systems, Beijing Institute of Technology, Beijing 100081, China.
[3] Key Laboratory of Biomimetic Robots and Systems, Ministry of Education, Beijing 100081, China.
[4] Department of Mechanical and Energy Engineering, Southern University of Science and Technology, Shenzhen 518055, China.
[5] Department of Mechanical Engineering, Tsinghua University, Beijing 100084, China.
[6] Human Biomechanics Laboratory, National Research Center for Rehabilitation Technical Aids, Beijing 100176, China.

in Fig. 1, the proposed method has been tested and performs impressive compliance which validates its effectiveness.

The remainder of the paper is organized as follows. Section II introduces the proposed compliance control method including the viscoelastic model definition and the compliance controller design. Section III describes how this method is used in stable walking on indefinite uneven terrain. Section IV presents the application in arm compliance for falling forwards protection. Section V presents the validation of the proposed method through experiment on BHR-6P. Section VI concludes the paper and introduces future work.

II. Compliance Controller Based on Viscoelastic Model

The viscoelastic model consists of elastic elements and viscous elements [14]. In this paper, we use a simple one, which has been used in our previous work [15], to design the compliance controller. In this section, we will firstly introduce the definition of the adopted viscoelastic model and the establishment of state equation. Afterwards, the compliance controller design based on state feedback and LQR method will be presented.

It is noted that the viscoelastic model and compliance controller presented in this section are generalized rather than specific. The model and controller can be used in both task and joint space, such as ankle compliance and arm joint compliance, the specific applications proposed in this paper, which will be presented in Section III and IV respectively.

A. Viscoelastic Model and State Equation

In order to adjust position according to force, we introduce a viscoelastic model to obtain the relationship between position and the differential of force. The adopted simple viscoelastic model with three elements is shown in Fig.2, which contains a parallel elastic element of stiffness $k1$, a parallel viscous element of viscosity b, and a series elastic element of stiffness $k2$, motivated by the well known three-element Hill muscle model in the biophysics domain [16].

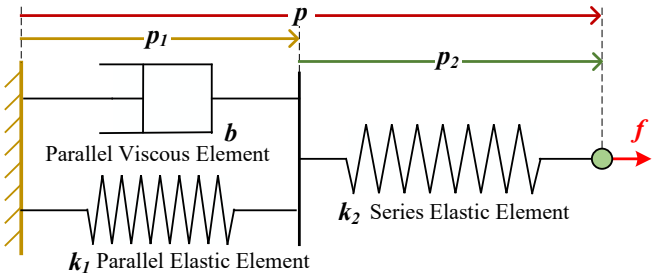

Fig. 2. The 3-element viscoelastic model used in this paper.

If there is external force f acted on the model, the corresponding strain (displacement) p and stress (internal force) $\sigma = -f$ would be produced. The parallel element strain p_1, series element strain p_2, and total strain p satisfy the equation

$$p = p_1 + p_2. \tag{1}$$

Then the total stress of this model is

$$\sigma = -f = k_1 p_1 + b\dot{p_1} = k_2 p_2. \tag{2}$$

Assuming that all initial values are zero, the Laplace transform for Eq. (2) is

$$f(s) = -k_1 p_1(s) - bsp_1(s) = -k_2 p_2(s). \tag{3}$$

From Eq. (3) we get

$$p_1(s) = -\frac{f(s)}{k_1 + bs}\ ,\ p_2(s) = -\frac{f(s)}{k_2}. \tag{4}$$

Substituting Eq. (4) into the Laplace transform of Eq. (1), we get the constitutive equation of the viscoelastic material as

$$f + \frac{b}{k_1 + k_2}\dot{f} = -\frac{k_1 k_2}{k_1 + k_2}p - \frac{k_2 b}{k_1 + k_2}\dot{p}. \tag{5}$$

The above equation represents the relationship between external force and displacement. Now we get the relationship between position and the first-order differential of force. Extended from [15], reformulating Eq. (5) and differentiating, we obtain

$$\begin{cases} \dot{f} = -\dfrac{k_1 + k_2}{b}f - \dfrac{k_1 k_2}{b}p - k_2\dot{p} \\ \ddot{f} = -\dfrac{k_1 + k_2}{b}\dot{f} - \dfrac{k_1 k_2}{b}\dot{p} - k_2\ddot{p} \end{cases}, \tag{6}$$

which also contains the second-order differential of force. Then we get an expression for the state space as

$$\frac{d}{dt}\begin{bmatrix} f \\ \dot{f} \\ p \\ \dot{p} \end{bmatrix} = \begin{bmatrix} -\frac{k_1+k_2}{b} & 0 & -\frac{k_1 k_2}{b} & -k_2 \\ 0 & -\frac{k_1+k_2}{b} & 0 & -\frac{k_1 k_2}{b} \\ 0 & 0 & 0 & 1 \\ 0 & 0 & 0 & 0 \end{bmatrix}\begin{bmatrix} f \\ \dot{f} \\ p \\ \dot{p} \end{bmatrix} + \begin{bmatrix} 0 \\ -k_2 \\ 0 \\ 1 \end{bmatrix}\ddot{p}. \tag{7}$$

According to this state equation, we can design a compliance controller using the state feedback control and LQR method. Other methods for obtaining feedback control gains can also be considered, such as pole placement. And the employment of new sate variable $\dot{f}$ introduces damping term in the feedback control of force making the controller more stably especially on multi-contact occasions than that in the previous work [15] where the state variables are $[f,\ p,\ \dot{p}]^T$.

B. Compliance Controller Design Using LQR Method

On the basis of Eq. (7), a state feedback controller is derived to track the desired force by modifying the acceleration of the end position $\ddot{p}$, which facilitates position compliance control. We rewrite Eq. (7) as

$$\dot{\boldsymbol{x}} = \boldsymbol{A}\boldsymbol{x} + \boldsymbol{B}\boldsymbol{u}, \tag{8}$$

where $\boldsymbol{x} = [f,\ \dot{f},\ p,\ \dot{p}]^T$, $\boldsymbol{u} = \ddot{p}$, $\boldsymbol{A}$ is the state matrix, and $\boldsymbol{B}$ is the input matrix. There is the same formulation for desired states and inputs:

$$\dot{\boldsymbol{x}}^d = \boldsymbol{A}\boldsymbol{x}^d + \boldsymbol{B}\boldsymbol{u}^d, \tag{9}$$

where $\boldsymbol{u}^d = \ddot{p}^d$ represents the desired acceleration obtained by motion generator such as Center of Mass (CoM) trajectory generator for walking and arm joint trajectory generator for falling protection in this paper.

Subtracting the expression in Eq. (9) from the expression in Eq. (8), we get a new formulation of the difference between actual and desired values as

$$\Delta\dot{\boldsymbol{x}} = \boldsymbol{A}\Delta\boldsymbol{x} + \boldsymbol{B}\Delta\boldsymbol{u}. \tag{10}$$

The state feedback controller is then given by

$$\Delta\boldsymbol{u} = -\boldsymbol{\kappa}\Delta\boldsymbol{x}, \tag{11}$$

where $\boldsymbol{\kappa} = [\kappa_1, \kappa_2, \kappa_3, \kappa_4]^T$, which can be obtained through the LQR method.

In order to get the feedback gains $\boldsymbol{\kappa} \in \mathbb{R}^{1\times 4}$, we firstly define the quadratic cost function as

$$J = \int_0^\infty (\Delta\boldsymbol{x}^T\boldsymbol{Q}\Delta\boldsymbol{x} + \Delta\boldsymbol{u}^T\boldsymbol{R}\Delta\boldsymbol{u})dt, \tag{12}$$

where $\boldsymbol{Q} = diag\{\omega_{\Delta f}, \omega_{\Delta \dot{f}}, \omega_{\Delta p}, \omega_{\Delta \dot{p}}\}$ is the weight matrix for the states and $\boldsymbol{R} = \omega_{\Delta \ddot{p}}$ is the weight matrix for the input. Substituting Eq. (11) into Eq. (12) yields

$$J = \int_0^\infty \Delta\boldsymbol{x}^T(\boldsymbol{Q} + \boldsymbol{\kappa}^T\boldsymbol{R}\boldsymbol{\kappa})\Delta\boldsymbol{x}dt. \tag{13}$$

Let $\boldsymbol{\kappa} = \boldsymbol{R}^{-1}\boldsymbol{B}^T\boldsymbol{P}$, where $\boldsymbol{P}$ can be obtained by solving the algebraic Riccati equation:

$$\boldsymbol{A}^T\boldsymbol{P} + \boldsymbol{P}\boldsymbol{A} - \boldsymbol{P}\boldsymbol{B}\boldsymbol{R}^{-1}\boldsymbol{B}^T\boldsymbol{P} + \boldsymbol{Q} = \boldsymbol{0}. \tag{14}$$

We then can get the values of feedback gains. The more specific position compliance controller has the formulation

$$\Delta\ddot{p} = -\kappa_1(f - f^d) - \kappa_2(\dot{f} - \dot{f}^d) - \kappa_3(p - p^d) - \kappa_4(\dot{p} - \dot{p}^d). \tag{15}$$

In actual application, the differences between the desired and actual values of position and velocity can be replaced by Δp and $\Delta\dot{p}$ which are initialized as 0 and calculated by integration such as

$$\begin{cases} \Delta\dot{p} = \Delta\dot{p} + T\Delta\ddot{p} \\ \Delta p = \Delta p + T\Delta\dot{p} \end{cases}, \tag{16}$$

where T is the discrete time of control system. Considering Eq. (16), the controller is given by

$$\Delta\ddot{p} = -\kappa_1(f - f^d) - \kappa_2(\dot{f} - \dot{f}^d) - \kappa_3\Delta p - \kappa_4\Delta\dot{p}. \tag{17}$$

C. Compliance Control Framework Based on Viscoelastic Model

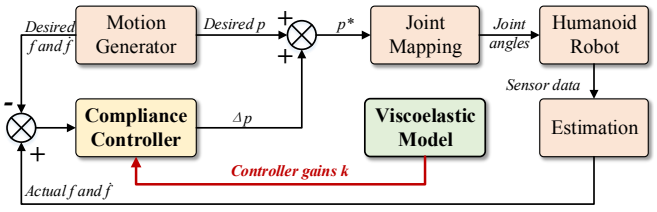

Fig. 3. Framework of compliance controller based on viscoelastic model.

The compliance controller works in the control system of a position-controlled humanoid robot as shown in Fig. 3. The motion generator provides the desired position p^d and desired force $f^d, \dot{f}^d$. The actual force $f, \dot{f}$ are obtained through sensor data and estimation, which will be introduced specifically for both ankle and arm joint compliance in later chapters. According to the differences between the desired and actual values, the compliance controller, the gains of which is calculated based on a predefined viscoelastic model, gives the modification of position as Δp. Then the new position command for a position-controlled robot is $p^* = p^d + \Delta p$, which will be mapped to joint position command by inverse kinematics in task space or direct mapping in joint space.

In this section, the situation of the viscoelastic model based compliance in 1-D space about position p and force f is introduced, while there is no difference when involving the situation of angle θ and torque τ.

III. Ankle Compliance Control for Stable Walking on Indefinite Uneven Terrain

The compliance control method is employed as ankle compliance control in the stable walking on indefinite uneven terrain, where the unknown obstacles may cause unexpected large contact impact resulting in serious instability. In addition, a CoM stabilization is also employed to restrain the disturbance caused by the impact. In this section, we will introduce the ankle compliance controller design and then briefly describe the pattern generation and stabilization for the stable walking.

A. Ankle Compliance Controller Design

The viscoelastic model is applied to the ankle of the humanoid robot as shown in Fig. 4. For ankle compliance during walking, we employ one linear and two angular viscoelastic models in the control of each ankle. The linear viscoelastic model is used for translation DoFs along the z axis as shown in Fig. 4(a). The angular viscoelastic models are adopted for rotational DoFs around the x and y axes as shown in Fig. 4(b)–(c) shows.

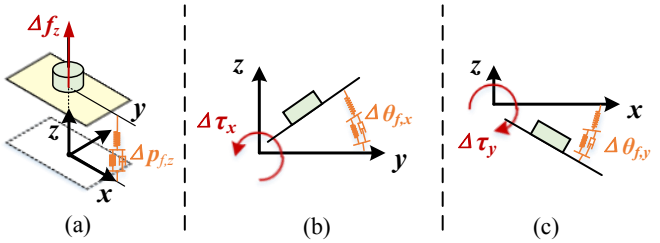

Fig. 4. Viscoelastic models applied to the ankle. (a) Vertical direction (translation along z axis); (b) Roll direction (rotation along x axis); (c) Pitch direction (rotation along y axis).

According to Eq. (17), the ankle compliance controller for position p and orientation θ, corresponding to contact force f and torque τ respectively, is therefore given by

$$\begin{cases} \Delta\ddot{\theta}_r = -\kappa_{r,1}(\tau_r - \tau_r^d) - \kappa_{r,2}(\dot{\tau}_r - \dot{\tau}_r^d) - \kappa_{r,3}\Delta\theta_r - \kappa_{r,4}\Delta\dot{\theta}_r \\ \Delta\ddot{\theta}_p = -\kappa_{p,1}(\tau_p - \tau_p^d) - \kappa_{p,2}(\dot{\tau}_p - \dot{\tau}_p^d) - \kappa_{p,3}\Delta\theta_p - \kappa_{p,4}\Delta\dot{\theta}_p \\ \Delta\ddot{p}_z = -\kappa_{z,1}(f_z - f_z^d) - \kappa_{z,2}(\dot{f}_z - \dot{f}_z^d) - \kappa_{z,3}\Delta p_z - \kappa_{z,4}\Delta\dot{p}_z \end{cases}, \tag{18}$$

where the subscripts r and p denote roll and pitch respectively.

In Eq. (18), the actual torque and force, τ_r, τ_p, and f_z, are obtained by the force/torque sensor mounted between the ankle and foot sole. The desired force and torques are decided by the walking pattern generator, meanwhile the torques will be modified by a posture feedback controller based on inverted pendulum with the modification $\Delta\tau_r^d$ and $\Delta\tau_p^d$ to maintain the upper body posture as presented in [15]. These modifications will be distributed into each ankle according to the actual force distribution in the vertical direction as

$$\begin{cases} \Delta\tau_{i,Left}^d = \dfrac{f_{z,Left}}{f_{z,Left}+f_{z,Right}}\Delta\tau_i^d \\ \Delta\tau_{i,Right}^d = \dfrac{f_{z,Right}}{f_{z,Left}+f_{z,Right}}\Delta\tau_i^d \end{cases}, \ i \in \{r,p\}. \quad (19)$$

The first-order differential of desired torques, $\dot{\tau}_p^d$ and $\dot{\tau}_r^d$, will be modified as well as $\dot{\tau}_p$, $\dot{\tau}_r$, $\dot{f}$, and $\dot{f}_z^d$ by forward difference method with limiting filters.

According to Eq. (16), the modification of double feet trajectory is

$$\begin{cases} \Delta\dot{\theta}_{r,i} = \Delta\dot{\theta}_{r,i} + T\Delta\ddot{\theta}_{r,i}, & \Delta\theta_{r,i} = \Delta\theta_{r,i} + T\Delta\dot{\theta}_{r,i} \\ \Delta\dot{\theta}_{p,i} = \Delta\dot{\theta}_{p,i} + T\Delta\ddot{\theta}_{p,i}, & \Delta\theta_{p,i} = \Delta\theta_{p,i} + T\Delta\dot{\theta}_{p,i} \\ \Delta\dot{p}_{z,i} = \Delta\dot{p}_{z,i} + T\Delta\ddot{p}_{z,i}, & \Delta p_{z,i} = \Delta p_{z,i} + T\Delta\dot{p}_{z,i} \end{cases}, \quad (20)$$

where $i \in \{Left,\ Right\}$. Then the trajectory of double feet will be adjusted as

$$\begin{cases} \theta_{r,i}^* = \theta_{r,i}^d + \Delta\theta_{r,i} \\ \theta_{p,i}^* = \theta_{p,i}^d + \Delta\theta_{p,i} \\ p_{z,i}^* = p_{z,i}^d + \Delta p_{z,i} \end{cases}, \ i \in \{Left,\ Right\}. \quad (21)$$

B. Walking Trajectory Generation and CoM Stabilization

The methods used for stable walking on indefinite uneven terrain mainly consists of walking pattern generation and CoM stabilization besides ankle compliance control.

In this work, we adopt 3-D Divergent Component of Motion (DCM) and Virtual Repellent Point (VRP) to generate the CoM trajectory of walking pattern [15], [17]. In 3-D space, the VRP $\boldsymbol{\gamma}$, DCM $\boldsymbol{\xi}$, and CoM $\boldsymbol{x}_c$ should satisfy

$$\ddot{\boldsymbol{x}}_c = (\boldsymbol{x}_c - \boldsymbol{\gamma})/b^2, \quad (22)$$

$$\dot{\boldsymbol{\xi}} = (\boldsymbol{\xi} - \boldsymbol{\gamma})/b, \quad (23)$$

$$\dot{\boldsymbol{x}}_c = -(\boldsymbol{x}_c - \boldsymbol{\xi})/b, \quad (24)$$

where $b = \sqrt{z_c/g}$, z_c is the height of the CoM from the contact surface.

As presented in [17], the DCM, also known as Capture Point (CP) [18], is defined as a point at a certain distance in front of the CoM and Eq. (24) shows a stable first-order dynamics about these two points which means the CoM will move towards the DCM. Considering Eq. (22) equivalent to

$$\boldsymbol{F} = m\ddot{\boldsymbol{x}}_c = m(\boldsymbol{x}_c - \boldsymbol{\gamma})/b^2, \quad (25)$$

where m is the mass of particle, the VRP can be defined as a point encoding the sum of all forces $\boldsymbol{F}$ acted on the CoM.

From Eq. (23), there is

$$\boldsymbol{\xi}(t) = \boldsymbol{\gamma} + e^{t/b}(\boldsymbol{\xi}(0) - \boldsymbol{\gamma}), \quad (26)$$

based on which we can obtain the initial DCM $\boldsymbol{\xi}_{ini,i}$ of every step i with a given step time T_{step} when the VRP in Single Support (SS) phase $\boldsymbol{\gamma}_i^{SS}$ is constant locating at the center of footholds and in the final step N it is defined that $\boldsymbol{\xi}_{end,N} = \boldsymbol{\gamma}_N^{SS}$. Introducing a period T_{DS} for Double Support (DS) pahse, the initial and last DCM of DS phase, $\boldsymbol{\xi}_{ini,i}^{DS}$ and $\boldsymbol{\xi}_{end,i}^{DS}$, as well as the trajectory of DCM in SS phase $\boldsymbol{\xi}_i^{SS}(t)$ can be obtained by Eq. (26). In DS phase, the DCM trajectory $\boldsymbol{\xi}_i^{DS}(t)$ is achieved via polynomial interpolation using $\boldsymbol{\xi}_{ini,i}^{DS}$ and $\boldsymbol{\xi}_{end,i}^{DS}$. The VRP trajectory in DS phase $\boldsymbol{\gamma}_i^{DS}(t)$ can be calculated by Eq. (23). Afterwards, we get the DCM and VRP trajectory, $\boldsymbol{\xi}(t)$ and $\boldsymbol{\gamma}(t)$. According to Eq. (24), the CoM trajectory $\boldsymbol{x}_c(t)$ is generated as well. In addition, the swing and support foot trajectories will be obtained by polynomial interpolation method.

Beside the walking pattern generator, a CoM stability controller based on VRP and DCM trajectory tracker established through output feedback method [15] is used together with the ankle compliance controller. The CoM stability controller in one dimension is as follows

$$\begin{cases} \Delta\dddot{x}_c = -K_1(\gamma - \gamma^d) - K_2(\xi - \xi^d) - K_3\Delta x_c \\ \qquad\qquad - K_4\Delta\dot{x}_c - K_5\Delta\ddot{x}_c \\ \Delta\ddot{x}_c = \Delta\ddot{x}_c + T\Delta\dddot{x}_c \\ \Delta\dot{x}_c = \Delta\dot{x}_c + T\Delta\ddot{x}_c \\ \Delta x_c = \Delta x_c + T\Delta\dot{x}_c \end{cases}, \quad (27)$$

where $K_1 \sim K_5$ are controller gains obtained based on the following state and output equations

$$\begin{aligned} \dot{\boldsymbol{X}} &= \boldsymbol{A}\boldsymbol{X} + \boldsymbol{B}\boldsymbol{U} \\ \boldsymbol{Y} &= \boldsymbol{C}\boldsymbol{X} \end{aligned}, \quad (28)$$

where $\boldsymbol{X} = [x_c, \dot{x}_c, \ddot{x}_c]^T$, $\boldsymbol{Y} = [\gamma, \xi, x_c, \dot{x}_c, \ddot{x}_c]$, and $\boldsymbol{U} = \dddot{x}_c$, are respectively the state, output, and input vectors. Furthermore,

$$\boldsymbol{A} = \begin{bmatrix} 0 & 1 & 0 \\ 0 & 0 & 1 \\ 0 & 0 & 0 \end{bmatrix}, \ \boldsymbol{B} = \begin{bmatrix} 0 \\ 0 \\ 1 \end{bmatrix}, \ \boldsymbol{C} = \begin{bmatrix} 1 & 0 & -b^2 \\ 1 & b & 0 \\ 1 & 0 & 0 \\ 0 & 1 & 0 \\ 0 & 0 & 1 \end{bmatrix}. \quad (29)$$

The modified CoM trajectory is then $\boldsymbol{x}_c^* = \boldsymbol{x}_c^d + \Delta\boldsymbol{x}_c$ obtained by the integration of CoM jerk increment $\Delta\dddot{\boldsymbol{x}}_c$ as Eq. (27) shows.

IV. Arm Joint Compliance Control for Falling Forwards Protection

In falling forwards protection, the proposed compliance control method is used to generate compliant movement for arm joints to deal with the large impact caused by the sudden contact in order to avoid robot hardware damage, which facilitates a more safe landing than our pervious work [19]

using only leg and waist movements. In this section, the application of viscoelastic model and compliance controller to the arm will be presented firstly. After that, other important algorithms, such as impact estimation, used in falling control will be introduced.

A. Arm Joint Compliance Controller Design

As shown in Fig. 5, the viscoelastic model is applied to the arms in joint space instead of cartesian space, and 3 angular viscoelastic models are employed for each arm according to the DoF configuration of BHR-6P. The viscoelastic models and compliance controllers applied to left and right arms have no difference, so we will introduce the application of one arm in the follows.

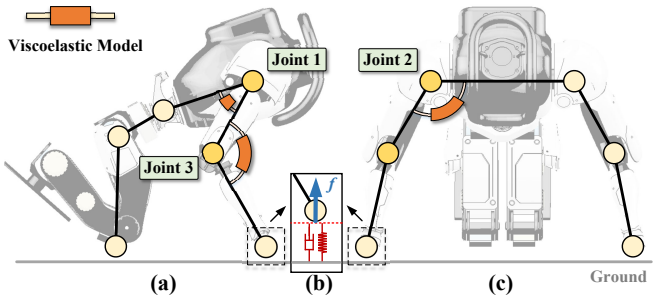

Fig. 5. Viscoelastic models applied to arm joints for compliance control and virtual spring-damping model for impact estimation. (a) Viscoelastic models applied to joint 1 and 3 of arm in pitch direction; (b) Virtual spring-damping model for impact estimation; (c) Viscoelastic model applied to joint 2 of arm in roll direction.

When the robot hand hit the ground, the impact force will be sensed and mapped to joint space by Jacobian matrix as

$$\boldsymbol{\tau} = \boldsymbol{J}^T \boldsymbol{F}, \tag{30}$$

where $\boldsymbol{\tau} = [\tau_1, \tau_2, \tau_3]^T$ denotes the impact torques of arm joints, $\boldsymbol{J}$ is the Jacobian matrix of arm, and $\boldsymbol{F}$ represents the impact force. According to Eq. (17), the arm joint compliance controller for joint angles $\boldsymbol{q} = [q_1, q_2, q_3]$ is therefore given by

$$\begin{cases} \Delta\ddot{q}_i = -\kappa^a_{i,1}(\tau_i - \tau^d_i) - \kappa^a_{i,2}(\dot{\tau}_i - \dot{\tau}^d_i) \\ \qquad\quad -\kappa^a_{i,3}\Delta q - \kappa^a_{i,4}\Delta\dot{q} \\ \Delta\dot{q}_i = \Delta\dot{q}_i + T\Delta\ddot{q}_i \qquad\qquad , i \in \{1,2,3\}, \\ \Delta q_i = \Delta q_i + T\Delta\dot{q}_i \\ q^*_i = q^d_i + \Delta q_i \end{cases} \tag{31}$$

where $\boldsymbol{\kappa}^a_i = [\kappa^a_{i,1}, \kappa^a_{i,2}, \kappa^a_{i,3}, \kappa^a_{i,4}]^T$ is the controller gains for ith joint, and τ^d_i is the desired torque. In the arm compliance control, we set $\tau^d_i = 0$ to achieve a compliant movement, while it could also be adjusted by some other controllers.

B. Falling Forwards Protection Realization

The falling forwards protection method mainly contains protective trajectory off-line optimization [19], impact force estimation, and arm compliance control.

In this paper, we use the Inertial Measurement Unit (IMU) to obtain the kinematic information of robot to detect the falling and calculate hand positions for impact force estimation. When the falling is detected and the protective motion is triggered, the joint trajectory obtained by off-line optimization will be executed. In the optimization, the humanoid robot is simplified as two models in different falling phases, which are telescopic inverted pendulum with flywheel before the knee contacting with ground, and inverted pendulum with flywheel and fixed length after the knee landing. Using this strategy, the impact force on the chest of a humanoid robot was reduced by 24% compared with a single dynamic model based off-line optimization strategy. More details could be found in our previous work [19].

Generally, the force sensor used on humanoid robots are easily damaged by large impact during falling. Thus we use a virtual spring-damping model and kinematics estimation based impact force estimation method instead of force sensor measurement to obtain the impact force which would be mapped to the arm joints to touch off compliant arm protective behaviour. In this work, the robot hands are equipped with gloves with low friction to make the hands slide when contacting with the ground, thus we only consider the impact force in vertical direction.

As shown in Fig. 5 (b), a virtual spring-damping model is assumed to be mounted between the hand and ground. During the arm cushioning process, the humanoid robot's knees are in contact with the ground, so we assume that the ground position equals the knee position. According to the torso posture angle, torso angular velocity, actual joint angles and angular velocities of the whole body, we can obtain the actual hand position h_{hand} and velocity $\dot{h}_{hand}$ relative to the ground (knee) in the vertical direction. Then, the impact force F is obtained by

$$F = -Kmin(h_{hand} - h_0, 0) - Bmin(\dot{h}_{hand}, 0) \tag{32}$$

where K, B, and h_0 represent the stiffness, damping, and the original length of the virtual spring-damping model. We can set $h_0 > 0$ to obtain the virtual impact force before hand contact with the ground; therefore, the arm compliance can be enabled slightly ahead of the time when a strong hand-to-ground impact occurs, which improves the robustness of the arm compliance control method and cannot be realized by force sensor detection. In addition, there is only compression force and no tension force between the hand and ground during the contact, which means $F \geq 0$, so we use $min(h_{hand} - h_0, 0)$ and $min(\dot{h}_{hand}, 0)$ to replace the normal form $h_{hand} - h_0$ and $\dot{h}$ in the virtual force calculation.

V. Experiments and Results

The proposed method has been validated on the BHR-6P, a position controlled humanoid robot, and performs stable walking on indefinite uneven terrain as well as safe landing during falling forwards.

A. Platform

As reported in the literature [15], the BHR-6P humanoid robot (Fig. 6) has a mass of 50 kg and 21 degrees of freedom comprising three in each arm, six in each leg, and

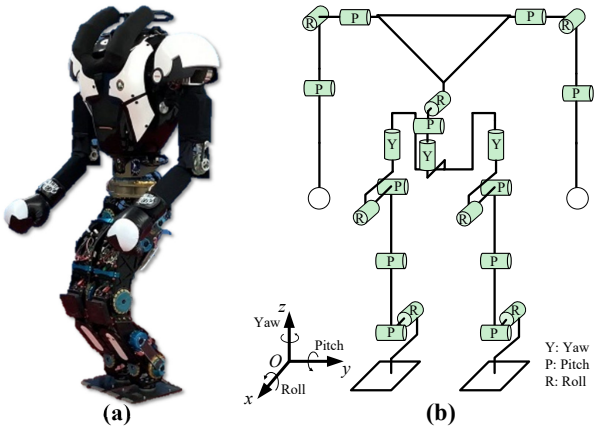

Fig. 6. BHR-6P humanoid robot platform. (a) Actual robot with cushion material on hands, knees, and chest; (b) Configuration of DoFs.

three in the waist. Each joint is driven by a brushless DC motor in a position control manner. A six-axis IMU sensor is mounted at the center of the torso to measure the posture and acceleration of the robot body. Additionally, there are two six-axis force/torque sensors mounted between the ankle and foot of each leg to obtain force/torque information.

B. Experiments

In order to validate the effectiveness of the proposed compliance control method based on viscoelastic model, walking and falling experiments were executed on BHR-6P. Tab. I shows the weight matrix of state and input for compliance controller design using LQR method.

TABLE I

LQR WEIGHT MATRIX OF COMPLIANCE CONTROLLERS FOR EXPERIMENT.

Compliance Controller	Weight Matrix	Value
All	$\boldsymbol{Q}$	$diag([1,1\ \ ^4,1,1])$
Ankle position	$\boldsymbol{R}_{p_z}$	[500]
Ankle pitch	$\boldsymbol{R}_{\theta_p}$	[20]
Ankle roll	$\boldsymbol{R}_{\theta_r}$	[20]
All arm joints	$\boldsymbol{R}_{Arm}$	[100]

In experiments shown in Fig. 7, the ankle compliance control based on viscoelastic model was demonstrated. In Fig. 7 (a), the robot was lifted with the ankle compliance controller on at first (Fig. 7 (a)-1), and then was put down with one foot contact with an obstacle, which is about $2.5cm$ high and unknown by the robot motion generator(Fig. 7 (a)-2). Under the control of the proposed method, the robot successfully adapted to the unknown obstacles and kept stable standing on the ground due to the vertical ankle compliance (Fig. 7 (a)-3). When the robot was lifted up again, the foot recovered at the same time (Fig. 7 (a)-4∼5).

In Fig. 7 (b), the robot stably walked through an unknown obstacle ($2.5cm$ high) at a speed of $1.35km/h$. The robot firstly stepped onto a part of the obstacle (Fig. 7 (b)-2),

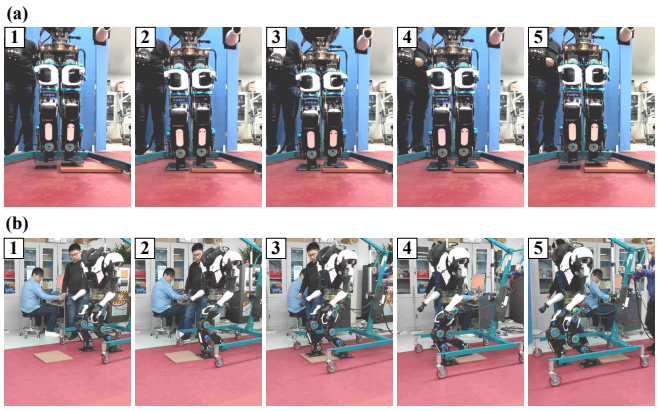

Fig. 7. Ankle compliance control experiment. (a) Ankle compliance controller test in vertical direction; (b) Walking on indefinite uneven terrain.

and the ankle compliance in pitch direction figured out the inclination which may cause instability. And in next step, the robot stably walked through the obstacle by vertical compliance which reduced the unexpected contact impacts(Fig. 7 (b)-3∼5).

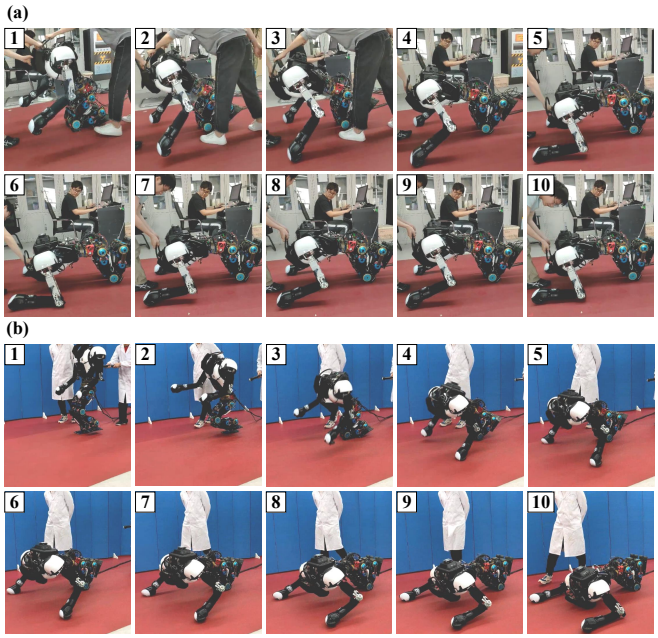

Fig. 8. Arm joint compliance control experiment. (a) Arm joint compliance controller test; (b) Falling forward protection with arm buffering.

The compliance controller employed in falling protection was tested as Fig. 8 shows. We firstly tested the compliance of arm motion as shown in Fig. 8 (a). In the test, the robot had contacted with the ground on knees, then we hold the robot and lifted it down to the ground (Fig. 8 (a)-1). It shows that the arm could compliantly move as the robot was lifted up or down(Fig. 8 (a)-2∼10) under the control of joint compliance controller and the impact force estimation.

In Fig. 8 (b), the compliance controller was demonstrated through actual falling forwards experiment. In Fig. 8 (b)-1∼3, the robot was pushed on the back and the protection

method was triggered. In Fig. 8 (b)-1, the hand of robot contacted with the ground, and the compliance controller started to act. From 8 (b)-1$\sim$10, we could find that the speed of the robot's torso was reduced and finally the robot lay on the round stably without any damage to hardware.

The above experiments show that the proposed compliance controller based on viscoelastic model is effective, and can be used to improve stability or protect hardware for humanoid robots.

VI. Conclusion

This paper presents a compliance control method based on viscoelastic model for position-controlled humanoid robots to overcome large impacts caused by unexpected or sudden contacts in complicated environment, which has been validated in the stable walking on indefinite uneven terrain and falling forwards protection on BHR-6P. In the future, we will expand the configuration of the viscoelastic model and introduce the adaptive control method to realize online adjustment of the controller gains, which may contribute to the improvement of dynamic complex environmental adaptability for humanoid robots.

References

[1] M. Kim, J. Oh, "Posture control of a humanoid robot with a compliant ankle joint," *International Journal of Humanoid Robotics*, vol. 7, no. 1, pp. 5-29, Mar. 2010.

[2] J. A. Castano, C. Zhou, Z. Li, N. Tsagarakis, "Robust model predictive control for humanoids standing balancing," in *Proc. IEEE Int. Conf. on Advanced Robotics and Mechatronics (ICARM)*, Macau, China, Aug. 18-20, 2016, pp. 147-152.

[3] S. Kajita, K. Yokoi, M. Saigo, and K. Tanie, "Balancing a humanoid robot using backdrive concerned torque control and direct angular momentum feedback," in *Proc. IEEE Int. Conf. Robot. Autom. (ICRA)*, Seoul, Korea, May 21-26, 2001, pp. 3376-3382.

[4] S. Kajita, M. Morisawa, K. Miura, S. Nakaoka, et. al.,"Biped walking stabilization based on linear inverted pendulum tracking," in *Proc. IEEE/RSJ Int. Conf. Intell. Robot. Syst. (IROS)*, Oct. 18-22, 2010, pp. 4489-4496.

[5] C. Ott, R. Mukherjee, and Y. Nakamura, "Unified impedance and admittance control," in *Proc. IEEE Int. Conf. Robot. Autom. (ICRA)*, Anchorage, USA, May 3-8, 2010, pp. 554-561.

[6] K. Nagasaka, M. Inaba, H. Inoue, "Stabilization of dynamic walk on a humanoid using torso position compliance control," in *Proc. of 17th Annual Conference on Robotics Society of Japan*, pp.1193-1194, 1999 (in Japanese)

[7] K. Nagasaka, "Whole-body motion generation for a humanoid robot by dynamics filters," PhD thesis, 1999, the Univ. of Tokyo, in Japanese.

[8] S. Caron, A. Kheddar, O. Tempier, "Stair climbing stabilization of the HRP-4 humanoid robot using whole-body admittance control," in *Proc. IEEE Int. Conf. Robot. Autom. (ICRA)*, Montreal, Canada, May 20-24, 2019, pp. 277-283.

[9] Y. Wang, R. Xiong, Q. Zhu, J. Chu, "Compliance control for standing maintenance of humnaoid robots under unknown external disturbances," in *Proc. IEEE Int. Conf. Robot. Autom. (ICRA)*, Hong Kong, China, May 31-June 7, 2014, pp. 2297-2304.

[10] S. Hyon, J. G. Hale, G. Cheng, "Full-body compliance human-humanoid interaction: balancing in the presence of unknown external forces," *IEEE Trans. Robot.*, vol. 23, no. 5, pp. 884-898, Oct. 2007.

[11] C. Ott, B. Henze, G. Hettich, et. al. "Good posture, good balance: comparison of bioinspired and model-based approaches for posture control of humanoid robots," *IEEE Robot. Autom. Mag.*, vol. 23, no. 1, pp. 22-33, Mar. 2016.

[12] O. Stasse, T. Flayols, R. Budhiraja, et. al., "TALOS: A new humanoid research platform targeted for industrial applications" in *Proc. IEEE-RAS Int. Conf. Humanoid Robots (Humanoids)*, Birmingham, UK, Nov. 15-17, 2017, pp. 689-695.

[13] PAL, "TALOS - Torque Controlled Balancing," 2018. [Online]. Available: https://www.youtube.com/watch?v=lX6Q0zgFut0

[14] P. Bawa, A. Mannard, R. B. Stein, "Predictions and experimental tests of a visco-elastic muscle model using elastic and inertial loads," *Biological Cybernetics*, vol. 22, pp. 139-145, Feb. 1976.

[15] Q. Li, Z. Yu, X. Chen, et. al., "Contact force/torque control based on viscoelastic model for stable bipedal walking on indefinite uneven terrain," *IEEE Trans. Autom. Sci. Eng.*, vol. 16, no. 4, pp. 1627-1639, Oct. 2019.

[16] A. V. Hill, "The heat of shortening and the dynamic constants of muscle", *Proceedings of the Royal Society of London B: Biological Sciences*, vol. 126, no. 843, pp. 136-195, 1938.

[17] J. Englsberger, C. Ott, A. Albu-Schäffer, "Three-dimensional bipedal walking control based on divergent component of motion," *IEEE Trans. Robot.*, vol. 31, no. 2, pp. 355-368, Apr. 2015.

[18] J. Pratt, J. Carff, S. Drakunov, A. Goswami, "Capture point: A step toward humanoid push recovery," in *Proc. IEEE-RAS Int. Conf. Humanoid Robots (Humanoids)*, Genova, Italy, Dec. 4-6, 2006, pp. 200-207.

[19] Q. Li, Z. Yu, X. Chen, et. al., "A falling forwards protection strategy for humanoid robots," in *Proceeding of ROMANSY 22 Robot Design, Dynamics and Control*, Rennes, France, June 25-28, 2018, pp. 314-322.